Clim Dyn (2008) 31:435–447
DOI 10.1007/s00382-007-0317-y

Simulated interannual variation in summertime atmospheric circulation associated with the East Asian monsoon

Miki Arai · Masahide Kimoto

Received: 16 October 2006 / Accepted: 6 September 2007 / Published online: 8 November 2007

Abstract The reproducibility of the interannual variability of the summertime East Asian circulation is examined using an atmospheric general circulation model (AGCM). An ensemble experiment is conducted using observed sea surface temperature (SST) of recent 20 years as a lower boundary condition. The spatial pattern associated with the first principal mode of observation of geopotential height at 500 hPa is characterized by a meridional wavy pattern extending over eastern Siberia, the vicinity of Japan and the subtropical western Pacific. The principal component (PC) time series of the leading mode is represented well by a high-resolution version of the AGCM with horizontal resolution T106 and with 56 vertical levels (T106L56), while with a lower resolution version, T42 and 20 vertical levels, the reproducibility is considerably degraded. The reproducibility by the AGCM suggests the importance of SST as a boundary condition. However, the simulated interannual variations show the alternating appearance of two distinct circulation regimes, a *cold summer regime* and a *hot summer regime*, exhibiting interesting bimodality in probability density distribution in PC phase space. This implies that the system's response to the continuously varying boundary condition includes nonlinearity. The nature of this nonlinearity is suggested to be wave breaking in the westerly region of the high latitudes that requires high resolution for the reproduction. Using the T106L56 model, another ensemble experiment was carried out with doubled CO_2. The climate change appears as an increase in residence frequency of the *cold summer regime* of the principal patterns of the present-day climate.

This paper is a contribution to the AMIP-CMIP Diagnostic Subproject on General Circulation Model Simulation of the East Asian Climate, coordinated by W.-C. Wang.

M. Arai (✉) · M. Kimoto
Center for Climate System Research, University of Tokyo, 5-1-5, Kashiwanoha, Kashiwa, Chiba 277-8568, Japan
e-mail: arai@ccsr.u-tokyo.ac.jp

1 Introduction

Summertime East Asian climate is substantially influenced by the intensity and the meridional position of the East Asian summer monsoon (EASM) front, which is observed as an extratropical rain band elongated from South China to the western Pacific, and is regarded as a part of the East Asian monsoon (e.g., Ninomiya and Murakami 1987). The rainband lies between the two anticyclones, which develop from early summer.

One of these anticyclones, the western Pacific subtropical high, plays a primary role in influencing the East Asian summer monsoon front because the southwesterly located western periphery of the high brings warm moist air from the low latitudes. Thus, many studies of the EASM front or the summertime East Asian climate have been dedicated to investigating the effect from the south, the tropical and subtropical Pacific. The convective activities in the tropical western Pacific influence the East Asian monsoon circulation and western Pacific subtropical high via Rossby wave propagation, and it is pointed out that they have a close relationship with El Nino-Southern Oscillation (ENSO; Nitta 1987; Huang and Sun 1992; Nitta and Hu 1996; Wu et al. 2003). Moreover, the intrerannual variation of the meridional position of the EASM front is influenced by sea surface temperature anomalies related to ENSO (Tomita et al. 2004).

In addition to the important influences from the south, the Okhotsk high located to the north of the EASM front has also been regarded as an important factor for the interannual variation of the EASM front (Kurashima 1969; Wang 1992). This northern anticyclone has an equivalent barotropic structure in most of the upper troposphere and is closely related to a blocking anticyclone over eastern Siberia and the Sea of Okhotsk. The Okhotsk high brings a cold northeasterly surface wind, called Yamase in Japanese, to the northeastern Japan when it is active (Ninomiya and Mizuno 1985; Kodama 1997). Thus, the development of the summertime Okhotsk high or blocking anticyclone is an important factor for anomalous cold summer in Japan. The eastward propagation of Rossby wave along the polar frontal jet, which develops in early summer by a strengthened meridional temperature gradient between Eurasian landmass and the Arctic Ocean, is essential for formation of blocking anticyclone over eastern Siberia and the Sea of Okhotsk (Wang and Yasunari 1994; Nakamura and Fukamachi 2004). It is also pointed out that the surface temperature over Siberia is closely correlated with the activity of blocking anticyclone (Tachibana et al. 2004; Arai and Kimoto 2005).

The observational trend for the last half of the 20th century of EASM rainfall shows the increase in central China and the decrease in northern China (Yatagai and Yasunari 1994; Hu et al. 2003). Hu et al. (2003) also pointed out that the future prediction of summertime Asian continental precipitation by coupled general circulation models (CGCM) has some uncertainty. However, intensification of the rain band elongated from Japan to the western Pacific, which is accompanied by East Asian summer monsoon, has shown in an ensemble of 17 CGCM (Kimoto 2005) and the high resolution atmospheric general circulation model (AGCM; Kusunoki et al. 2006) under the influence of global warming. Many of the results of global warming projection by CGCMs also show large increases in surface temperature over the continents (the latest results can be seen in the IPCC Data Distribution Centre website; http://www.ipcc-ddc.cru.uea.ac.uk). This means that summertime land–sea temperature contrast increases, and it is inferred that monsoonal circulation over East Asia is intensified (IPCC 2001). However, there is little agreement so far on the future summertime East Asian climate, which is predicted by different CGCMs (Giorgi et al. 2001).

In this study, we investigate the possibility of reproducing the interannual variability of the summertime East Asian climate using a relatively high resolution AGCM. The climate change due to global warming is also examined by the AGCM in association with the present-day interannual variations.

2 Experiments and data

The model used in this study is the atmosphere and land components of the CCSR/NIES/FRCGC coupled climate model, MIROC (K-1 model developers 2004). The resolution is spectral T106 truncation in horizontal and 56 vertical levels. This horizontal resolution corresponds to a 125 km grid size on the equator. To represent the interannual variation of the present climate, a five-member ensemble experiment is performed; each run of the experiment is integrated from different initial conditions, while the same observed sea surface temperature (SST) and sea ice concentration from January 1979 to December 1998 are used as boundary conditions. To investigate the resolution dependence of the reproducibility of the summertime East Asian circulation, a three-member ensemble experiment is also performed under the same boundary condition except with a model horizontal resolution T42 and 20 levels in the vertical. Another ensemble experiment with resolution T106L56 under the doubled CO_2 condition is performed to simulate climate change due to global warming. The SSTs used for these integrations are evaluated as observed SST from 1979 to 1998 plus climatological increments by global warming for each month, which are estimated by seven kinds of CGCMs (see Inatsu and Kimoto 2005 for detail). The experiments under the present-day CO_2 concentration with the horizontal resolution T106 and T42 are referred to as PD_hi and PD_mid, respectively while we call the experiment under the doubled CO_2 condition $2CO_2$, hereafter.

The observational dataset used for diagnosing PD_hi and PD_mid is the European Centre for Medium–Range Weather Forecasts 40-year re-analysis (ECMWF ERA-40). Only for precipitation, we used Climate Prediction Center merged analysis of precipitation (CMAP) compiled by the National Oceanic and Atmospheric Administration, Cooperative Institute for Research in Environmental Sciences (NOAA-CIRES; Xie and Arkin 1997).

The model performance to represent the summertime East Asian monsoon is examined by a comparison with the observational climatology of precipitation in summer. The 20-year climatology of June–July–August (JJA) averaged precipitation of the observation and the models are shown in Fig. 1. The East Asian rain band that is observed from eastern China to northwestern Pacific (Fig. 1a) is not sufficiently represented by the simulation with T42 (Fig. 1c) as pointed out by Kang et al. (2002). On the other hand, in the climatology of AGCM with T106 (Fig. 1b), precipitation over the Korea and Japan is enhanced as large as the observation although the EASM rain band is not extended to the east as that of observation. This dependency of the representation of the East Asian rain band on the horizontal resolution of AGCM has also been pointed out by Kawatani and Takahashi (2003) and Kusunoki et al. (2006).

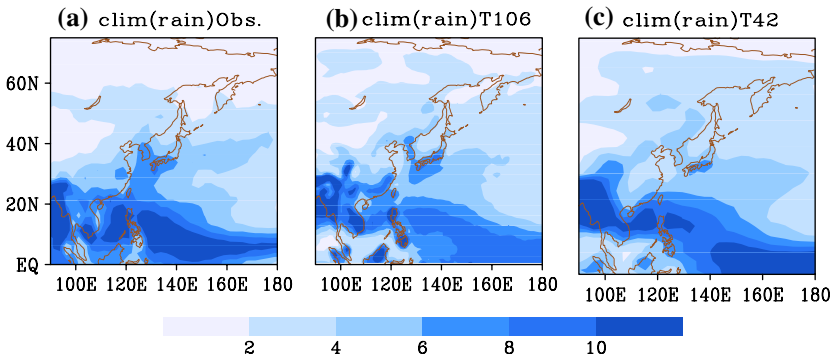

Fig. 1 Climatology of JJA precipitation for 20 years (1979–1998). Contour interval is 2 mm/day. **a** The observation from CMAP, **b** AGCM with horizontal resolution T106, and **c** AGCM with horizontal resolution T42

3 The summertime leading EOF modes

To assess the extent to which the model can represent the current interannual variation of the summertime East Asian climate, we inspect JJA averaged geopotential height anomaly at the 500 hPa level, over the East Asia and the western North Pacific area (80°E–160°E, 20°N–70°N). We perform an empirical orthogonal function (EOF) analysis for 20 summers for the observation and for 20 × 5 summers of the PD_hi experiment. The anomaly of PD_hi is defined as difference between JJA-mean value for each year of each run and that for 20-year climatology of the five-member ensemble average.

Figure 2 shows linear regression maps of the 500 hPa geopotential height (Fig. 2a, b), and those of precipitation and sea level pressure (c, d) against the first principal component (PC1) time series (Fig. 2e). This mode explains 35.0 and 31.2%, for observation and PD_hi, respectively, of the total variance. The regressed patterns correspond to ones for unit standard deviation of PC1, and the time series plotted in Fig. 2e is normalized. Characteristics of the EOF1 spatial patterns of observation and PD_hi are quite

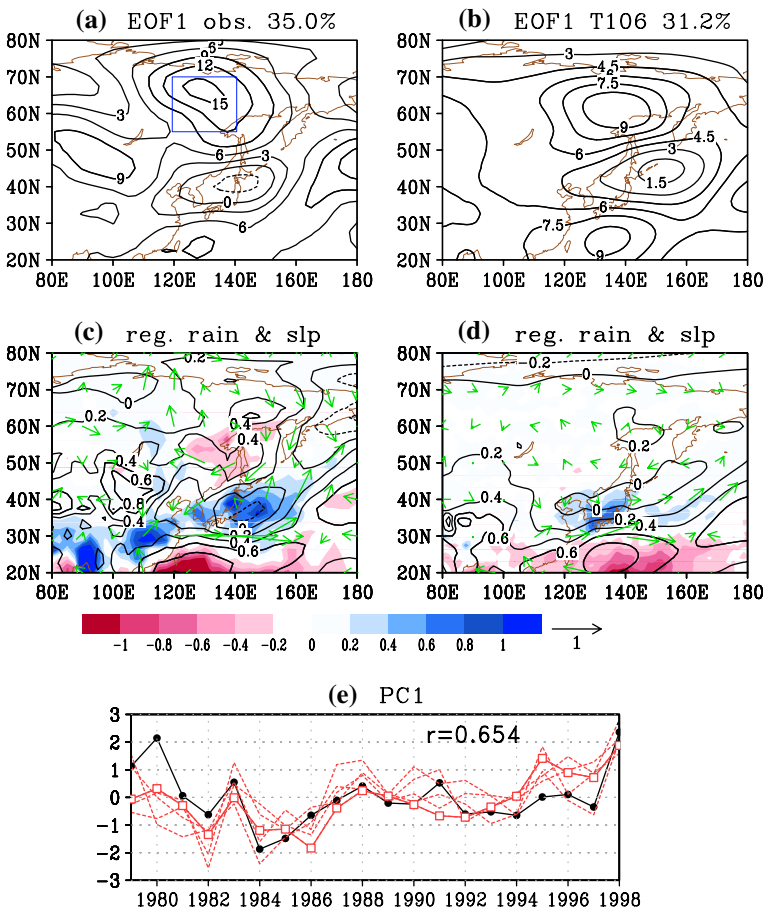

Fig. 2 The regressed patterns of PC1 with geopotential height at the 500 hPa level (**a** and **b** Contour intervals are 3.0 and 1.5, respectively), precipitation (**c** and **d** *shaded*. Contour intervals are 0.2. *Blue shades* denote positive and red is negative), sea level pressure (**c** and **d** contour. Contour intervals are 0.2) and the 850 hPa wind (**c** and **d**). The left-hand column is for ERA-40, while the right-hand column is for PD. **e** Time series of PC1 for ERA-40 (*black solid line*) and for PD (*red broken lines* each members of ensemble, *red solid line* ensemble mean). Time series are normalized by each standard deviation

similar (Fig. 2a, b); a meridional wavy structure, consisting of anomaly centers over high- and low-latitudes and opposite sign region over mid-latitude, is dominant over the East Asia and over the western Pacific. This mode accompanies an enhanced rain band from South China to the western Pacific (Fig. 2c, d), corresponding to the region of negative height anomaly in 30°N–40°N as depicted in Fig. 2a and b. Moreover, it is remarkable that interannual variation of this mode is faithfully reproduced by the AGCM. Most of the timing of peaks of the PC1 time series of PD_hi corresponds with that of observation (Fig. 2e); the correlation coefficient of PC1 between observation and PD_hi ensemble mean is 0.65. This principal mode consists of an anomaly in the Okhotsk high area over east Siberia and the Sea of Okhotsk and the subtropical Pacific-Japan (P-J) pattern, as its spatial pattern shows. The correlation coefficient between PC1 and an index to represent the interannual variation of blocking activity over east Siberia and the Sea of Okhotsk, defined as an area average of geopotential height at 500 hPa over 120°E–140°E, 55°N–70°N (the area shown as blue rectangular in Fig. 2a), is 0.52 for observation and 0.38 for PD_hi. On the other hand, the correlation between PC1 and area averaged outgoing long wave radiation (OLR) over the subtropical western Pacific area (145°E–150°E, 15.7°N–20°N) which is a source region of P–J pattern (Nitta 1987) is 0.52 and 0.39 for observation and PD_hi, respectively. The correlation coefficients of PC1, with the geopotential height over eastern Siberia and with northwestern Pacific OLR attain the 99% significance for observation and PD_hi. Thus, the two distinctive features of the summertime interannual variation in East Asia could be extracted as the first principal mode.

The spatial pattern of the second EOF mode is characterized by a dipole structure between high- and mid-latitudes (Fig. 3a, b). Waves are zonally elongated and the contrast between positive and negative anomaly centers is larger than that of the first mode. The positive zone of 30°N–45°N corresponds to a dry area as shown in Fig. 3b and d. The correlation coefficient of PC2 between observation and PD_hi is again relatively high, 0.50 (exceeds the 99% significance level). Therefore, we conclude that the East Asian interannual variability represented by this AGCM is sufficiently realistic. Moreover, these two modes must be strongly influenced by boundary conditions, such as SST. Spatial patterns of the leading modes show that an influence upon the summertime East Asian rain band is from the north, in addition to the subtropical monsoonal

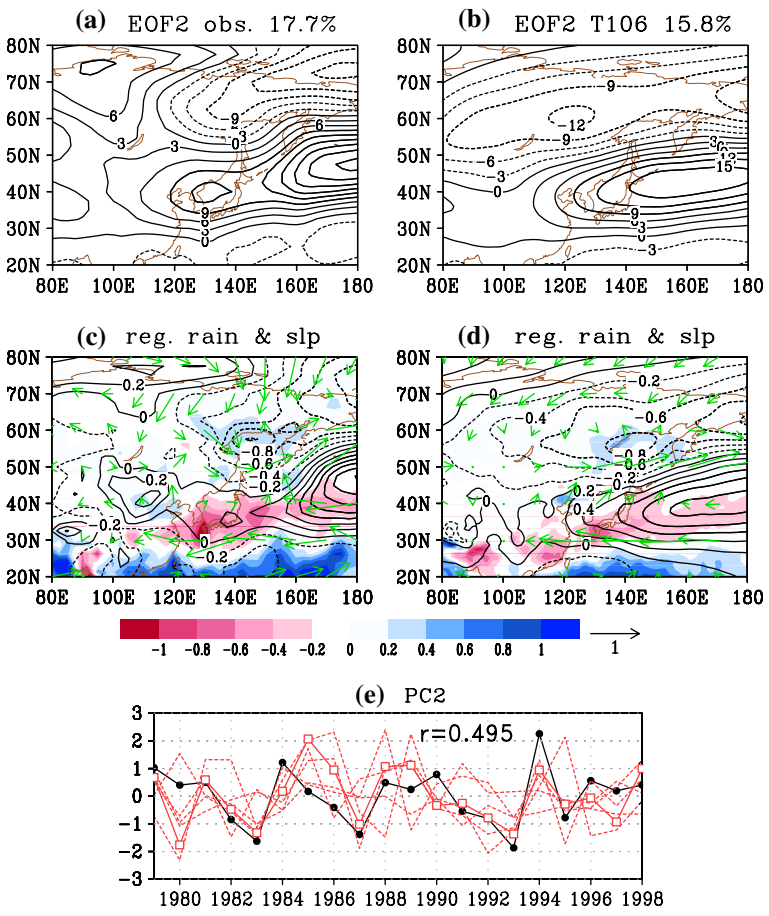

Fig. 3 Same as Fig. 1 but for PC2

flow, which has been pointed out as key factor of the interannual variation of the EASM front (Ninomiya and Murakami 1987). The characteristics of spatial pattern and the PC1 time series of the principal modes did not change when the reference domain used for the EOF analysis was varied and when the rotated EOF analysis was applied.

The use of lower resolution degrades the similarity to observations. Figure 4 shows the regressed spatial pattern and time series associated with the first and second EOF mode of PD_mid experiment. The center of action over northeastern Siberia, which is a prominent feature on the spatial pattern of EOF1 derived from observation and PD_hi ensemble experiment (Fig. 2a, b), move to the west to the central Siberia as seen in Fig. 4a. The center of action in high latitude also exists over the Kamchatka which lies to the southeast of the center of action of the observation and PD_hi. The middle- and low-latitude centers are reasonably simulated although the centers of action are located to the north of the original latitude. The correlation coefficient between the PC1 time series (Fig. 4e) of the ensemble mean and that of the observation is 0.32 with 90% significance. The spatial pattern of the second principal mode is similar to that of observation (Fig. 4b), but, the correlation coefficient between the PC2 time series of PD_mid and that of the observation is −0.19 (Fig. 4f). The experiment of PD_mid does not represent the connection between the principal modes and lower boundary conditions, in contrast with PD_hi.

4 Relationship between principal modes and SST variation

The PC1 time series of all ensemble members of the high-resolution PD experiment have very similar characteristics to that of the observed PC1 as shown in Fig. 2e. This means that the prescribed boundary condition controls the summertime principal pattern over East Asia to a large extent. The global surface temperature anomaly associated with the first EOF mode of the present-day interannual variability is depicted in Fig. 5 in order to understand which areas are related to the principal mode of PD; geopotential height on the 500 hPa level and 2 m temperature regressed against PC1 of observation (a) and PD_hi (b) and PD_mid (c) are shown. Since the air temperature near the sea surface is forced by SST as the boundary condition, 2 m temperature should reflect the local SST variation. In fact, the variability of 2 m temperature was equivalent to that of SST.

The position of warm surface temperature anomaly over the Eurasian Continent corresponds to that of anticyclone; warm anomaly over the anticyclone which is a part of the meridional wavy structure over the Far East and the East

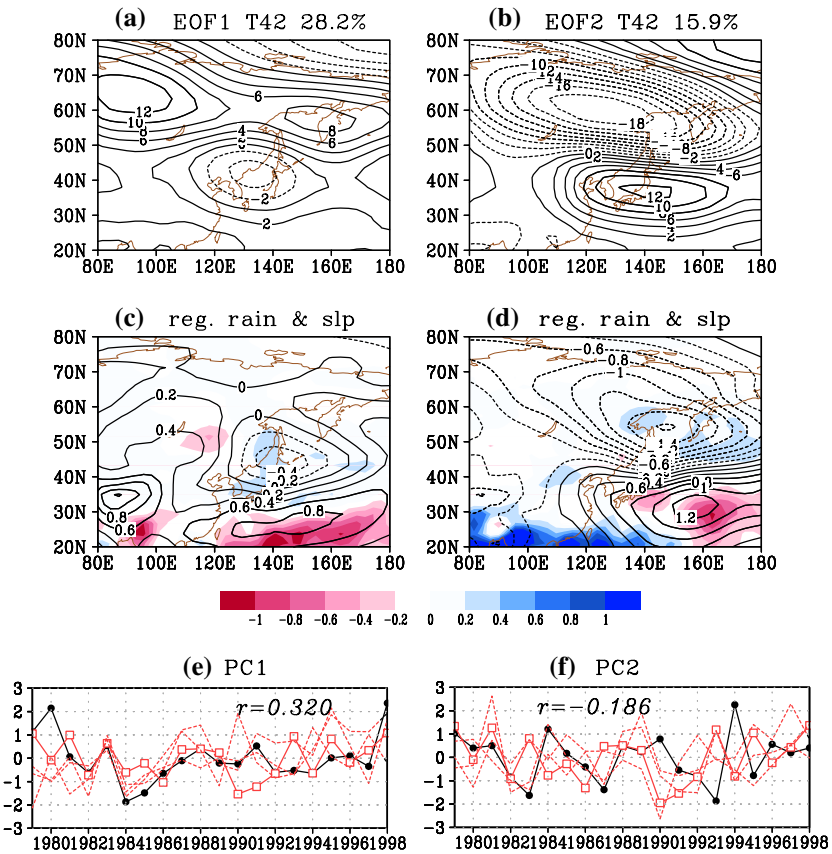

Fig. 4 Same as in Fig. 1 but for three-member ensemble experiment with T42. The regressed patterns of geopotential height at the 500 hPa level against PC1 is **a** and that for PC2 is **b**. The regression with precipitation and sea level pressure against PC1 (**c**) and that against PC2 (**d**). Time series of PC1 (**e**) and PC2 (**f**) for ensemble mean is depicted as a *red solid line* and those for three ensemble members are *red broken lines*. Time series of PC1 for ERA-40 are also shown as a *black solid line*. Time series are normalized by each standard deviation

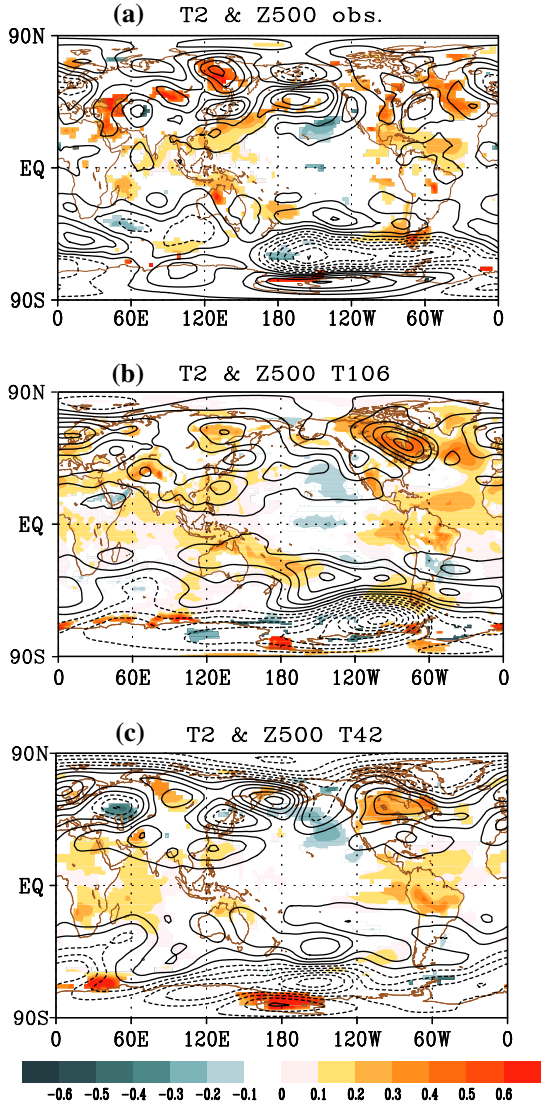

Fig. 5 The regression map of 2 m temperature (*shaded*) and 500 hPa geopotential height (*contour*) anomaly against PC1 for **a** ERA-40, **b** PD with T106 and **c** PD with T42. Only more than 90% significant areas are *shaded*

Asia associated with PC1 is particularly outstanding for observation and for PD_hi. On the other hand, the counterpart of PD_mid is not seen because the anticyclone is located to the east compared with observation. The regression pattern of the PD_hi resembles that of observation not only over the land surface but also over the ocean. The common feature of the subtropical Pacific surface temperature is a warm anomaly over the western subtropical Pacific and a cold anomaly over the central-eastern tropical Pacific. The SST anomalies of these areas influence the interannual variation of the EASM front and the East Asian monsoon (Nitta 1987; Lau et al. 2000). This result seems to conflict with Wang et al. (2005), who suggested that Asian summer monsoon rainfall is reproduced by coupled models because of the importance of local air–sea interaction in the tropical western North Pacific. However, as deduced from the meridional wavy structure, the spatial pattern associated with PC1 can be regarded as a remotely forced pattern. We further examine which determines the first principal mode later in this section.

The interannual variation of SST in the tropics is closely related to the local convective heating. The regressed patterns of OLR against PC1 are also depicted in Fig. 6. The tropical convective activities have the western Pacific subtropical dry (positive) and equatorial wet (negative) anomalies. The meridional dipole seen in the convective activity anomaly over the western Pacific is very similar to P–J pattern found by Nitta (1987). It is consistent with the high correlation coefficient between PC1 and convective activities over the subtropical western Pacific, which was mentioned in Sect. 3. The negative anomaly of OLR over the equatrial western Pacific is not apparent and subtropical positive anomaly is zonally elongated in the regressed pattern of PD_mid (Fig. 6c) compared with that of PD_hi. On the other hand, the intensity of the convective activities over the subtropical western Pacific is better simulated by PD_mid than PD_hi. However, the observed see–saw structure between the subtropics and the equatorial area over the western Pacific is well simulated by both of PD_hi and PD_mid models.

The large OLR anomalies associated with PC1 are restricted over the subtropics and tropics although the action center of the spatial geopotential pattern associated with PC1 extends to the high-latitude. Can the horizontal pattern associated with the first EOF mode be regarded as a remotely forced pattern? To understand the role of tropical and subtropical convective heating due to SST variations on the principal pattern of current interannual variation over the East Asia, we performed a linear response experiment. A linear model to estimate the steady response from tropical thermal forcing in this study is a dry linear baroclinic model of Watanabe and Kimoto (2000, 2001). As a prescribed forcing for the model, diabatic heating obtained by cumulus and large-scale condensation heating for each PD experiment with T106 and T42 and precipitation for observation, are given. The vertical profile of heating for observation is defined by an empirical function proposed by Reed and Recker (1971). A basic state is defined as the JJA mean of 20-year climatology for observation, while JJA-mean climatology of ensemble averages for the AGCM experiments with T106 and T42 are used for the linear response experiments with a corresponding resolution. The resolution of the linear model is T42 in horizontal and 20 levels in the vertical.

Figure 7 shows the prescribed thermal forcing and corresponding steady response of geopotential height on the

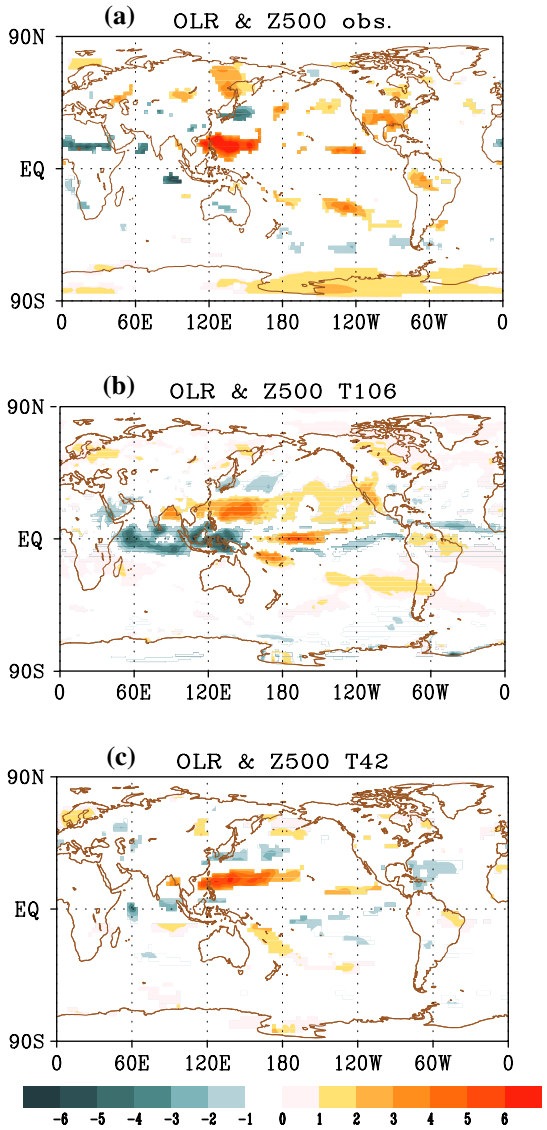

Fig. 6 The regression map of outgoing long wave radiation (*shaded*) and 500 hPa geopotential height (*contour*) anomaly against PC1 for **a** ERA-40, **b** PD with T106 and **c** PD with T42. Only more than 90% significant areas are *shaded*

500-hPa level obtained by the linear baroclinic model. The tripolar meridional wavy pattern that consists of subtropical ridge, mid-latitude trough, and high-latitude ridge can be seen in the response pattern to the observed forcing (Fig. 7b) and that to PD_hi (Fig. 7d). However, relative strength of the anticyclone in high latitude is much smaller than that shown in EOF pattern of observation and PD_hi. Moreover, the position of the anticyclone shifts southward. The mid-latitude negative center of PD_hi shifts westward, compared with the observation and PD_mid. The anticyclone in high latitude is not recognized in the response pattern from the T42 linear response experiment (Fig. 7f). The see–saw between the tropics and mid-latitude shifts to the north although the meridional position of the thermal forcing is not so different from those for observation and PD_hi. The northward shift of the see–saw is also seen in horizontal structure associated with PC1 of the PD_mid experiment (Fig. 4a). When the linear response experiment is performed with the thermal forcing of PD_mid and with the basic state of observation, an anticyclone over in high-latitude is not seem in the steady response of geopotential height. It is suggested from this result that the detailed expression of spatial structure of imposed forcing is essential to simulate the summertime East Asian circulation.

These results show that the summertime East Asian first EOF mode is almost regarded as a linear response from the thermal forcing in the subtropical western Pacific. However, as shown in Fig. 7a and b, the action center of the high latitude is not predominant compared with the action center of the principal pattern associated with PC1 (Fig. 1a, b). Moreover, the position of the northern action center of linear response pattern is located to the south of that of the first EOF pattern. It is possible that the interannual variation of the summertime East Asian first EOF mode is not simply determined by forcing from the subtropical western Pacific, especially for the northern part of the domain. In general, atmospheric nonlinearity is more important in the mid- and high-latitude than in the subtropics. An analysis from this point of view will be presented later.

5 The effect of global warming on summertime East Asian climate

5.1 Two regimes in the simulated East Asian circulation

In this section, we consider the summertime East Asian climate change due to global warming using $2CO_2$ experiment. First of all, 20-year climatology of $2CO_2$ and that of PD_hi are compared. Figure 8 shows the difference in climatology of JJA averaged 500 hPa geopotential height, 2 m temperature and precipitation between ensemble mean of $2CO_2$ and that of PD. Taking into account of the global rise of the 500 hPa surface due to warming, the difference of globally averaged climatology between PD and $2CO_2$ is subtracted from the 500 hPa geopotential field of $2CO_2$. Under the doubled CO_2 condition, surface temperature is preferentially increased over the northeastern Siberia and geopotential height on the 500 hPa over the northeastern Siberia and Sea of Okhotsk increases (Fig. 8a). Precipitation along the rain band from East Asia to the western Pacific becomes more pronounced (Fig. 8b) as previous studies have reported (Kimoto 2005; Kusunoki et al. 2006). The increase in rainfall over the western China is also similar to some results of global warming simulation (Hu et al. 2003; Bueh et al. 2003).

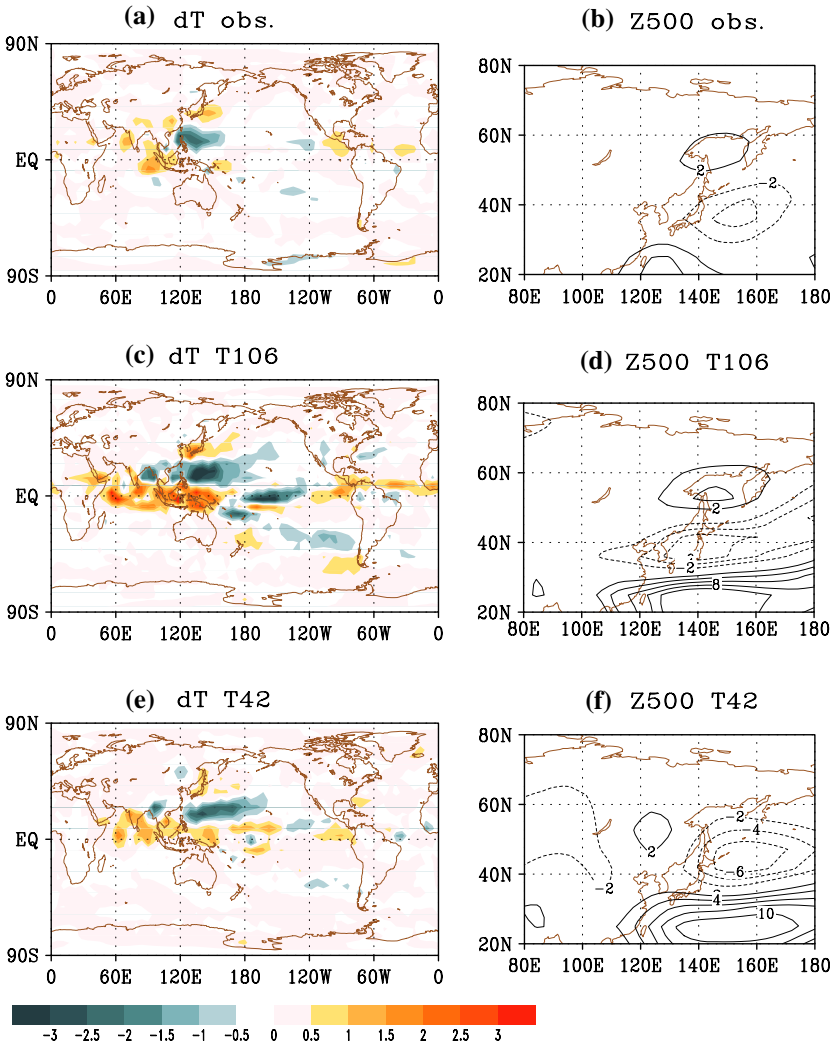

Fig. 7 The vertically averaged heating prescribed for linear baroclinic model (**a**, **c**, **e**) and steady response obtained by linear baroclinic model (**b**, **d**, **f**). The *top panels, middle panels, and lower panels* are obtained from regression against PC1 of ECMWF, PD, and PD with T42 model, respectively

We further examine how the interannual variation of summertime East Asian circulation changes due to global warming. In order to examine the change in the interannual variation, the characteristics of the interannual variation of PD_hi have to be clarified first. Samples of each month of all the ensemble members are mapped onto a two dimensional phase space extended by EOF1 and EOF2 of PD. The left hand panel of Fig. 9 shows the probability density function (PDF) of JJA monthly geopotential height of all the members of PD_hi. The value on the abscissa and the ordinate is standardized using the standard deviation of PC1.

The interannual variation of PD_hi exhibits interesting bimodality; i.e., two distinct regimes are found, which are discriminated by the sign of projection onto PC1. The geopotential anomaly field of positive PC1 case is characterized by the enhanced anticyclone over the Far East and over the western subtropical Pacific, and vice-versa. Moreover, there are positive temperature anomalies over eastern Siberia and negative temperature anomaly over northern part of East Asia in composite map with positive PC1, and vice-versa. Thus, the regime with positive PC1 will be called as *cold summer regime*, and that with negative PC1 as *hot summer regime* referring to surface temperature characteristics in the vicinity of Japan. The bimodal feature in PDF is not recognized very clearly in a similar figure for the observation (Fig. 8c). Note that number of samples used in the observed plot is one fifth of that of PD_hi and the variability of PDF estimation should be lower. However, a trace of weather regimes is seen; some isolated high probability density areas are distributed over the PC phase space, and the positions of some of them correspond to those of regimes for PD_hi.

5.2 Possible contributing factor for bimodality

Although the principal mode of the summertime East Asian circulation may be almost determined by interannual variability of tropical SST and convective activity, the influence of tropical SST anomalies on the northern anticyclone is

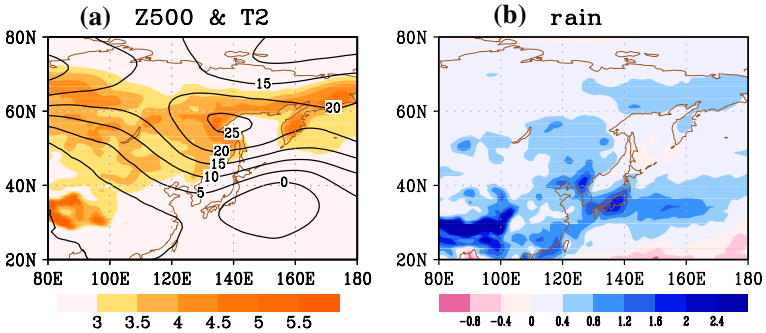

Fig. 8 The difference in 20-year climatology of JJA-mean (**a**) 2 m temperature (*shade*), geopotential height at the 500 hPa level (*contour*), and **b** the precipitation between seven-member ensemble mean of $2CO_2$ and five-member ensemble of PD

relatively weak according to the linear response experiment presented in the previous section. There must be a process other than the influence of the tropical and the subtropical SST anomalies in the development of the northern anticyclone. For example, the quasi-stationary Rossby wave propagation along the polar frontal jet, which is developed in summer, is one of the principal factors to develop blocking anticyclones over the East Siberia and the Sea of Okhotsk (Nakamura and Fukamachi 2004). An evolution of a blocking anticyclone can be seen as an irreversible mixing of the potential vorticity due to a breaking Rossby waves (Hoskins et al. 1985).

To clarify the role of the irreversible mixing process due to a Rossby wave breaking on the two distinct regimes, we compare the characteristics related to the quasi-stationary Rossby wave propagation for each regime. Since the intrinsic time scale of Rossby wave train is larger than that of synoptic eddies and less than a month, 11-day running averaged daily dataset is used to extract Rossby wave train and to subtract the synoptic disturbances. A phase-independent wave activity flux (Takaya and Nakamura 2001) is helpful to diagnose the statistical property of propagation of wave packets. A transient component of a potential vorticity flux $\mathbf{v}'q'$ is related to the time mean flow by the time mean potential vorticity equation without friction,

$$\frac{\partial \bar{q}}{\partial t} + \bar{\mathbf{v}} \cdot \nabla \bar{q} = -\nabla \cdot (\overline{\mathbf{v}'q'}) = -\left(\frac{\partial \overline{u'q'}}{\partial x} + \frac{\partial \overline{v'q'}}{\partial y} \right), \qquad (1)$$

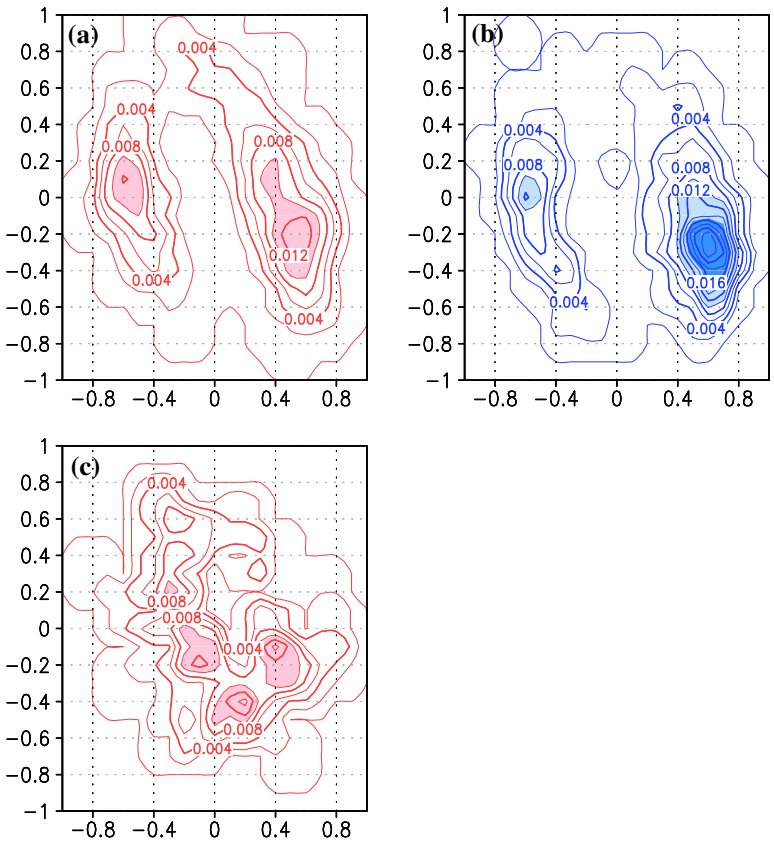

Fig. 9 Probability density function of PD_hi (**a**) and $2CO_2$ (**b**) in the phase space spanned by EOF1 and EOF2 of PD_hi. The PDF of observation is depicted in panel (**c**) as projection upon the observed EOFs. Contour intervals are 0.002 in all the panels. *Light shadings* denote exceeding 0.01 while heavy shadings exceeding 0.015

where $\overline{\mathbf{V}}$ and $\bar{q}$ are velocity and potential vorticity of mean flow, $\mathbf{v}' = (u',v')$ and q' the velocity and potential vorticity of the transient part. The overbar and prime in the equation are designated variables associated with the time mean flow and the transient, respectively. Here, we suppose mean flow to be a low-frequency field that varies with time scales more than a month, while the transient part is eddy with sub-monthly time scale, which is evaluated by 11-day running averaged daily dataset. Therefore, the composite of the transient part is made by figuring out the running averaged daily time series whose calendar month belongs to the *cold* or *hot summer regime*.

The difference between *cold* and *hot summer regimes* is depicted in Fig. 10 in which the panel (a) is a composite map with observation and (b) is that with PD_hi. Since *cold* and *hot summer regime* is defined on the basis of PC1 of observation, the months for making composites are only 9 and 8, respectively. On the other hand, composites with PD_hi are calculated for 81 months in *cold summer regime* and for 82 months in *hot summer regime*. Because the meridional component of the potential vorticity flux divergence (the latter term of the right hand side of (1)) is dominant over the zonal one, the horizontal pattern of the contribution from the meridional component of the potential vorticity flux is shown by shades in Fig. 10. According to Eq. 1, convergence of the transient vorticity flux makes a positive contribution to a time mean potential vorticity, and vice versa.

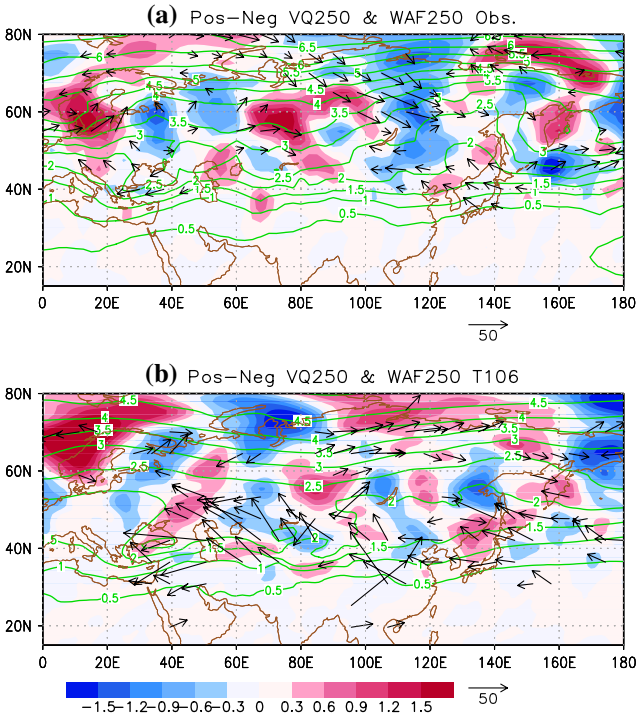

Fig. 10 The difference of wave activity flux (*arrow*) and meridional component of potential vorticity flux (*shade*) at the 250 hPa level between *cold summer* and *hot summer* regimes. The climatology of ensemble averaged potential vorticity in JJA is also depicted by *green solid lines*. The panel **a** is with observation and **b** with PD_hi

The feedback by the breaking Rossby waves can be seen in the observation albeit with limited sample size. In the both panels, the eastward anomaries of wave activity is dominant during *cold summer regime* from the central to eastern Siberia (80°E–140°E, 60°N–70°N) although the route of Rossby wave propagation for observation indicated by the wave activity flux is southeastward compared with that of PD_hi. Thus, more quasi-stationary Rossby waves propagate along the polar frontal jet, and the wave activity converges over the eastern Siberia during *cold summer regime*. The wave activity convergence that appears in composite map suggests that a Rossby wave breaking occurs more frequently during *cold summer regime* than during *hot summer regime*. Diffluence of the mean flow is seen in the climatological potential vorticity (green solid lines in Fig. 10), just downstream of the wave activity convergence in the area of 110°E–120°E, 50°N–60°N for observation and 130°E–140°E, 50°N–60°N for PD_hi. There is a negative potential vorticity flux, namely downgradient potential vorticity flux area, near the wave activity convergence area, located at 110°E–120°E, 50°N–70°N for observation and 130°E–140°E, 50°N–70°N for PD_hi. The downgradient transient potential vorticity flux accompanied with a convergence to the south and a divergence to the north reinforces the diffluence of the mean flow.

The possible feedback process from Rossby wave propagation over eastern Siberia to a diffluent flow is illustrated schematically in Fig. 11. When the mean flow with monthly to seasonal time scale is diffluent over eastern Siberia, potential vorticity anomaly is negative in the northern part of the diffluence and positive in the southern part. As can be seen in Fig. 10, downgradient meridional potential vorticity is dominant in the diffluence region. Thus, the negative anomaly in the north and the positive anomaly in the south of the diffluence are both enhanced. This means that the diffluence in the mean flow is amplified by the divergence/convergence of the transient potential vorticity flux associated with breaking Rossby waves. Therefore, once the system resides in one of regimes, it tends to and shows the distinct bimodality. This process is consistent with that the interannual variation of the East Asian circulation is determined by the prescribed SST. A similar feedback effect is well known during the formation and the maintenance of blocking flows over the northern Pacific and over the northern Europe from synoptic disturbances rather than quasi-stationary Rossby waves found in this study (Shutts 1983; Mullen 1987; Nakamura et al. 1997).

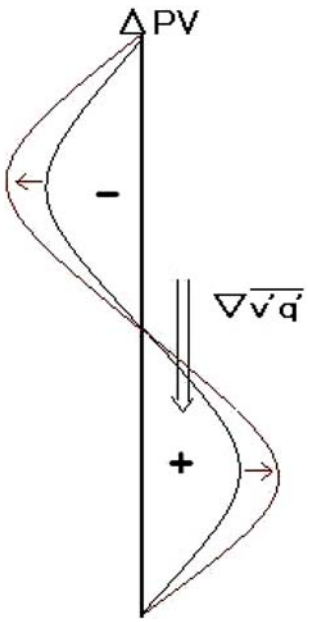

Fig. 11 Schematic diagram of the feedback process of meridional potential vorticity flux of transient eddies to potential vorticity anomaly of the mean flow. The abscissa is potential vorticity anomaly and the ordinate denotes latitude from 40°N to 70°N

The simulation of the wave breaking process should require high horizontal resolution. From this point of view, experiments with T106 model are advantageous over those with T42.

5.3 Change in the interannual variation due to global warming

We project the interannual variation of $2CO_2$ onto EOFs of PD to consider the change in the interannual variation under the global warming. Figure 9b is PDF projected on the phase space given by EOF1 and EOF2 of PD_hi. The residence probability in the *cold summer regime* of $2CO_2$ increases compared with that of PD, while that in the *hot summer regime* of $2CO_2$ decreases. As can be inferred from Fig. 7, the climatology of $2CO_2$ changes in the positive direction of the abscissa from PD, and the interannual variation of $2CO_2$ is shifted to prefer one side of weather regimes of the *cold summer*. It should be noted that the increase of the *cold summer regime* event is in a warmer background by global warming.

The climatological change in the geopotential field and precipitation by global warming owing to the CO_2 increase (Fig. 9), is caused by changes in the residence frequency of regimes of the present-day climate, as discussed by Palmer (1999) and Corti et al. (1999), although the principal mode in this study may not be a purely natural mode of atmosphere-only variability because of its correlation with SSTs. Palmer (1999) and Corti et al. (1999) discussed an AGCM experiment and observed tropospheric circulation during boreal winter. In addition, it is found in this study that the climate regime shift due to global warming exists also in the simulated summertime East Asian climate.

6 Discussion and conclusion

In this study, we succeeded in reproducing the interannual variation of summertime large-scale circulation over the East Asia of the present-day, using a relatively high resolution AGCM. The simulated interannual variation of summertime East Asian circulation shows distinct bimodality; *cold summer regime* and *hot summer regime* in Japan. The projection of the interannual variation under global warming onto the principal modes of PD shows that the residence of the *cold summer regime* becomes more frequent. This change in the appearance frequency of the regimes leads to the climatological enhancement of the anticyclone over the eastern Siberia and rain band along the EASM front. Such change in the residence frequency of regimes has been discussed by Palmer (1999) for natural variability using a simple climate model. It would be very interesting to examine the model dynamics, which causes such bimodal distribution of the summertime East Asian interannual variability. A clue to bimodality is given in this study. Since every member of the leading PC time series of PD_hi resembles much to the observed one, it is possible that the interannual variation of the seasonal mean can largely be considered as a response to the boundary condition, e.g., SST. This is in contrast to the previous general notion that the potential predictability of the summertime East Asian climate is not very high (Brankovic and Palmer 1997, 2000). Since this study is focused the eastern part of the EASM frontal rainfall and upper tropospheric circulation over the East Asia, we can reproduce the interannual variation of the summertime East Asian monsoon by AGCM. However, as Wang et al. (2005) pointed out, there is some incoherence in other parts of the Asian summer monsoon rainfall. For example, the rainfall pattern over the central and southwestern China that is apparent in EOF1 for the observation is poorly reproduced by AGCM_hi (Fig. 2a, b). The first principal pattern in this study is, as described in the Sect. 4, recognized as a teleconnection pattern forced by the subtropics. On the other hand, Wang et al. (2005) suggest that the Asian monsoonal rainfall is caused by local air–sea interaction. The discrepancy between the result of this study and that of Wang et al. (2005) can be due to whichever of a local or a remote forcing is paid attention.

In addition to the influence from the tropical western Pacific, the nonlinearity associated with Rossby wave

breaking in the westerly region of the high latitude may also play a key role in the interannual variation of the summertime principal pattern over East Asia. The composite of *cold summer regime* shows clear active Rossby wave propagation followed by wave breaking in the vicinity of large-scale diffluence, compared with that of *hot summer regime*. The substantial downgradient potential vorticity flux due to an enhanced Rossby wave breaking is shown over eastern Siberia; the northern negative anomaly and the southern positive anomaly of the low-frequency mean flow, which has from monthly to seasonal time scale, is enhanced by breaking Rossby waves. This positive feedback by breaking Rossby waves must contribute the bimodality in the simulated interannual variation of summertime East Asian circulation.

The interannual variation of the summertime East Asian principal mode is affected by the tropical western Pacific convection anomaly associated with tropical SST variability. The convective activity anomaly is very similar to that of P-J pattern (Fig. 6). It is also pointed out that P-J pattern has an intimate relationship to ENSO (Nitta 1987). The lag correlation coefficient between PC1 and SST anomaly in the previous winter of Nino3.4 area, which is defined as 5°N–5°S, 120°W–170°W is very high; 0.55 for observation and 0.46 for PD_hi. On the other hand, the simultaneous correlation during summertime is not significant; −0.18 for observation and 0.05 for PD. However, as shown in Fig. 5, SST over the west offshore of South America shows a meaningful positive anomaly; the correlation coefficient between PC1 and SST anomaly over the eastern part of the tropical Pacific (5°N–5°S, 80°W–120°W), attains the 95% significant level, 0.22 and 0.19, for the observation and for PD, respectively. The most of the climatology of prescribed SSTs for the $2CO_2$ experiments, which were evaluated by CGCMs under the doubled CO_2 condition, show El Nino-like change in the tropical eastern Pacific. The change in the tropical Pacific to El Nino is a key role of the change in the residence frequency to *cold summer regime*. Wang et al. (2000) mentions that the anomaly in subtropical wind over the western Pacific associated with wintertime ENSO is preserved until early summer. This seasonality of the impact from the ENSO calls for further investigation.

It is interesting that the surface temperature variations over the northeastern Siberia associated with the leading 500 hPa variability is also the common characteristics in the observation and PD_hi, although the land surface temperature is interactively calculated in PD_hi (Fig. 5a, b). A part of the surface temperature anomaly must be corresponding to the geopotential height anomaly however, it has already been mentioned in previous studies that a blocking anticyclone associated Okhotsk high is correlated well with surface temperature over the northeast Siberia (Nakamura and Fukamachi 2004; Tachibana et al. 2004; Arai and Kimoto 2005). This relationship between the high surface temperature anomaly and enhancement of an anticyclone over Siberia is consistent with the change due to global warming as shown in Fig. 8. Moreover, an AGCM experiment by Kimoto (2005; his Fig. 4) demonstrates that Siberian surface warming contributes to the strengthening of the downstream anticyclone. Summertime high surface temperature over Siberia can link the blocking anticyclone over the northeast Siberia as the following: when surface temperature over Siberia is high, a large meridional temperature gradient between the Arctic Ocean and the Eurasian Continent enhances the polar frontal jet which becomes a wave guide of quasi-stationary Rossby waves. Increased Rossby waves propagating along the polar frontal jet break over the eastern Siberia and positive feedback proposed in the Sect. 5 will be observed more frequently than usual. Further investigation is necessary to confirm whether the above process can be reproduced in an AGCM experiment. Moreover, the role of the surface temperature over eastern Siberia in the positive feedback between the diffluence in the mean flow and breaking Rossby waves would be clarified; whether the high surface temperature over Siberia is a only result of a warm air advection due to the anticyclone over the northeast Siberia or an precursor of blocking anticyclone incident to wave breaking.

Acknowledgments The authors appreciate the two anonymous reviewers for valuable suggestions. This study was supported by the Core Research for Evolutional Science and Technology of the Japan Science and Technology Agency, and by the Kyosei and Kakushin project of the ministry of education, culture, sports, science, and technology, and by the Global Environment Research Fund (GERF) of the Ministry of the Environment of Japan. All the figures were drawn by Grid Analysis and Display System (GrADS).

References

Arai M, Kimoto M (2005) Relationship between springtime surface temperature and early summer blocking activity over Siberia. J Meteorol Soc Japan 83:261–267

Bueh C, Cubasch U, Lin Y, Ji L (2003) The change of North China climate in transient simulation using the IPCC SRES A2 and B3 scenarios with a coupled atmosphere–ocean general circulation model. Adv Atmos Sci 20:755–766

Brankovic C, Palmer TN (1997) Atmospheric seasonal predictability and estimates of ensemble size. Mon Wea Rev 125:859–874

Brankovic C, Palmer TN (2000) Seasonal skill and predictability of ECMWF PROVOST ensembles. Q J Roy Meteorol Soc 126:2035–2067

Corti S, Molteni F, Palmer TN (1999) Signature of recent climate change in frequencies of natural atmospheric circulation regimes. Nature 398:799–801

Giorgi F, Whetton PH, Jones RG, Christensen JH, Mearns LO, Hewitson B, Von Storch H, Francisco R, Jack C (2001) Emerging patterns of simulated gerional climatic changes for

the 21st century due to anthropogenic forcings. Geophys Res Lett 28:3317–3320
Hu Z-Z, Yang S, Wu R (2003) Long-term climate variations in China and global warming signals. J Geophys Res 108:4614. doi: 10.1029/2003JD003651
Huang R, Sun F (1992) Impacts of the tropical western Pacific on the East Asian summer monsoon. Meteorol Soc Japan 70:243–256
Hoskins BJ, McIntyre ME, Robertson AW (1985) On the use and significance of isentropic potential-vorticity, maps. Q J Roy Meteorol Soc 111:877–46
Inatsu M, Kimoto M (2005) Two types of interannual variability of the mid-winter storm-tracks and their relationship to global warming. SOLA 1:61–64
IPCC (2001) Climate change 2001: the science of climate change. In: Houghton JT et al (eds) Cambridge University Press, New York, p 944
Kang I-S, Jin K, Wang B, Lau K-M, Shukla J, Krishnamurthy V, Schubert SD, Wailser DE, Stern WF, Kitoh A, Meehl GA, Kanamitsu M, Galin VY, Satyan V, Park C-K, Liu Y (2002) Intercomparison of the climatological variation of Asian summer monsoon precipitation simulated by 10 GCMs. Clim Dyn 19:383–395
Kawatani Y, Takahashi M (2003) Simulated of the Baiu front in a high resolution AGCM. Meteorol Soc Japan 81:113–126
K-1 model developers (2004) K-1 coupled GCM (MIROC) description. In: Hasumi H, Emori S (eds) K-1 Technical Report, *1*, 34 pp. (available from the Center for Climate System Research, University of Tokyo)
Kimoto M (2005) Simulated change of the East Asian circulation under the global warming Scenario. Geophys Res Lett 32:L16701. doi:10.1029/2005GL023383
Kodama Y-M (1997) Airmass transformation of the Yamase air-flow in the summer of 1993. Meteorol Soc Japan 75:737–751
Kurashima A (1969) Reports on Okhotsk high-report of the annual meeting on forecasting technique for the year 1966. J Meteorol Res 21:170–193
Kusunoki S, Yoshimura J, Yoshimura H, Noda A, Oouchi K, Mizuta R (2006) Change of Baiu rain band in global warming projection by an atmospheric general circulation model with a 20-km grid size. J Meteorol Soc Japan 63:581–611
Lau K-M, Kim K-M, Yang S (2000) Dynamical and boundary forcing characteristics of regional components of the Asian summer monsoon. J Clim 13:2461–2482
Mullen SL (1987) Transient eddy forcing of blocking flows. J Atmos Sci 22:3–22
Nakamura H, Fukamachi T (2004) Evolution and dynamics of summertime blocking over the Far East and the associated surface Okhotsk high. Q J Roy Meteorol Soc 130:1213–1234
Nakamura H, Nakamura M, Anderson JL (1997) The role of high- and low-frequency dynamics in blocking formation. Mon Weather Rev 125:2074–2093
Ninomiya K, Mizuno H (1985) Anomalously cold spell in summer over Northeastern Japan caused by northeasterly wind from polar maritime airmass. J Meteorol SocJapan 63:845–871
Ninomiya K, Murakami T (1987) The early summer rainy season (Baiu) over Japan. In: Chang C-P, Krishnamurti TN (eds) Monsoon meteorology. Oxford University Press, Oxford, pp 93–121
Nitta T (1987) Convective activities in the tropical western Pacific and their impact on the Northern Hemisphere summer circulation. J Meteorol Soc Japan 65:373–390
Nitta T, Hu ZZ (1996) Summer climate variability in China and its association with 500 hPa height and tropical convection. J Meteorol Soc Japan 74:425–445
Palmer TN (1999) A nonlinear dynamical perspective on climate prediction. J Clim 12:575–591
Reed RJ, Recker EE (1971) Structure and properties of synoptic-scale wave disturbances in the equatorial western Pacific. J Atmos Sci 28:1117–1133
Shutts GJ (1983) The propagation of eddies in diffluent jetstreams: eddy vorticity forcing of ''locking' flow fields. Q J Roy Meteorol Soc 109:737–761
Tachibana Y, Iwamoto T, Ogi M, Watanabe Y (2004) Abnormal meridional temperature gradient and its relation to the Okhotsk high. J Meteorol Soc Japan 82:1399–1415
Takaya K, Nakamura H (2001) A formulation of a phase-independent wave-activity flux for stationary and migratory quasigeostrophic eddies on a zonally varying basic flow. J Atmos Sci 58:608–627
Tomita T, Yoshikane T, Yasunari T (2004) Biennial and lower-frequency variability observed on the early summer climate in the western north Pacific. J Clim 17:4254–4266
Wang B, Ding Q, Fu X, Kang I-S, Jin K, Shukla J, Doblas-Reyes F (2005) Fundamental challenges in simulation and prediction of summer monsoon rainfall. Geophys Res Lett 32:L15711. doi: 10.1029/2005GL022734
Wang B, Wu R, Fu X (2000) Pacific-East Asian teleconnection: how does ENSO affect East Asian climate? J Clim 13:1517–1536
Wang Y (1992) Effects of blocking anticyclones in Eurasia in the rainy season (Meiyu/Baiu season). J Meteorol Soc Japan 70:929–951
Wang Y, Yasunari T (1994) A diagnostic analysis of the wave train propagating from high-latitudes to low-latitudes in early summer. J Meteorol Soc Japan 72:269–279
Watanabe M, Kimoto M (2000) Atmosphere–ocean thermal coupling in the North Atlantic: a positive feedback. Q J R Met Soc 126:733–734
Watanabe M, Kimoto M (2001) Corrigendum. Q J R Met Soc 127:929–951
Wu R, Hu Z-Z, Kirtman BP (2003) Evolution of ENSO-related rainfall anomalies in East Asia. J Clim 16:3742–3758
Xie P, Arkin PA (1997) Global precipitation: a 17-year monthly analysis based on gauge observations, satellite estimates, and numerical model outputs. Bull Am Meteorol Soc 78:2539–2558
Yatagai A, Tasunari T (1994) Trends and decadal-scale fluctuations of surface air temperature and precipitation over China and Mongolia during the recent 40 year period (1951–1990). J Meteorol Soc Japan 72:937–957